# Photoinduced Charge Separation of Pyrene in Chromium Containing Silicoaluminophosphate (SAPO-5) Microporous Materials at Room Temperature

**Koodali T. Ranjit* and Larry Kevan†**

*Department of Chemistry, University of Houston, Houston, Texas 77204-5003*

*Received: October 22, 2002*

The photoinduced charge separation of pyrene in chromium containing microporous SAPO-5 materials with ultraviolet irradiation at room temperature was examined. Photoionization of pyrene in Cr containing SAPO-5 results in the formation of pyrene cation radicals that are characterized by electron spin resonance (ESR) and diffuse reflectance spectroscopy (DRS). ESR studies indicate that Cr(V) acts as an electron acceptor. The photoyield and stability of the photoproduced pyrene cation radical were found to depend on the pore size of the microporous material, the concentration, and the oxidation state of chromium ions. The photoyield and stability of the photoproduced pyrene cation are found to be higher than in mesoporous materials investigated in our laboratory earlier. The study thus demonstrates the importance of Cr containing microporous SAPO-5 materials as potential candidates for photochemical conversion and storage devices.

## Introduction

Interest in designing molecular systems that can mimic photosynthesis is a subject that continues to attract the attention of several researchers.[1−3] An increased understanding of the photosynthetic process has made it possible to create artificial devices that can carry out functions of the natural process. Nature accomplishes its complex photosynthetic cycle by precise arrangement of each component so as to maximize the efficiency of each step.[4] The challenge lies in the design of systems in which all components of the energy conversion can be incorporated into a single material. Much of the effort has been devoted to the development of systems that can sustain charge separation long enough so that the free energy of the photoproduced cation (anion) can be utilized to drive a chemical reaction.[5] Once the initial photoinduced electron transfer is completed, there is a large driving force for the back electron transfer (BET) reaction and steps must be taken to minimize or eliminate this. The BET results in the loss of the stored energy of the photoproduced cation into heat. Thus, one of the main objectives is to design artificial photosynthetic systems in which long-lived charge separation can be achieved. Furthermore, it is also desirable to achieve this under ambient conditions of temperature and pressure.

A number of host systems have been examined to improve the efficiency of photoinduced charge separation by minimizing BET reaction.[6−8] Heterogeneous systems such as vesicles, micelles, silica gels, etc. have been reported to provide appropriate spatial organization of both donor and acceptor molecules to retard BET reaction.[9−14] By incorporating built-in donor/acceptor components, the electronic properties of the host system can be further tuned and BET can be further minimized. Thus, heterogeneous systems such as zeolites and microporous silicoaluminophosphates (SAPO) and mesoporous MCM-41 materials have been found to be promising hosts as compared to homogeneous systems.[15−18]

Extensive research has been done on zeolites as hosts for photoinduced charge separation.[19−21] Zeolites such as zeolite Y and zeolite X have often been a choice because their uniform and regular framework provides appropriate electronic and spatial environment to retard BET. The unique arrangement of channels and pores in its three-dimensional network allows for well-defined spatial arrangement of organic molecules. Aluminophosphates (AlPO-*n*) molecular sieves form a class of microporous crystalline material comparable to zeolites. The structure of AlPO covers a wide range of structure types; some are analogous to zeolites such as chabazite (AlPO-34), but there are a large number of AlPOs that are unique and have no zeolite analogue such as AlPO-5 and AlPO-11.[22] An interesting property of AlPO materials is that by incorporation of silicon atoms into the AlPO framework, SAPO materials are formed and ion exchange capacity can be introduced. Further modification of SAPO materials by incorporation of transition metal ions can have important implications in catalysis.[23]

SAPO-5 is composed of 4-ring, 6-ring, and 12-ring straight channels that are interconnected by 6-ring windows. The main channel is nearly circular and has a pore opening of 7.3 Å. In SAPO-11, the main channels are formed from 10 rings with an elliptical shape of 6.3 Å × 3.9 Å. SAPO-34 has the chabazite structure with ellipsoidal cages that can be accessed through 8-ring windows with 3.8 Å diameter. The structures of the SAPO materials used in the present study are depicted in Figure 1.

The photochemistry of polycyclic aromatic hydrocarbons (PAH) adsorbed on surfaces has received considerable attention.[24] The photochemistry of PAH adsorbed on several oxide materials such as silica and alumina has been reported.[25−27] These studies have important applications in the field of environmental chemistry since many of the PAH have been classified as priority pollutants by the EPA. Pyrene, a typical example of PAH, is often the popular choice due to its unique photophysical and photochemical properties. The ionization potential of pyrene is 7.55 eV in the gas phase, and the photoionization of pyrene leads to the formation of pyrene cation radical. Electron spin resonance (ESR) identifies the paramagnetic property of the cation radical ($Py^{+\bullet}$) whereas diffuse reflectance and luminescence spectroscopies provide valuable information regarding the physisorption and/or chemisorption

† Deceased June 4, 2002.

10.1021/jp022284a CCC: $25.00 
Published on Web 02/13/2003

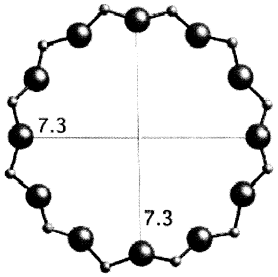


(a) SAPO-5 structure, 12-ring viewed along 001

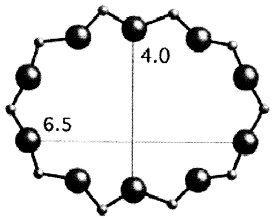


(b) SAPO-11 structure, 10-ring viewed along 001

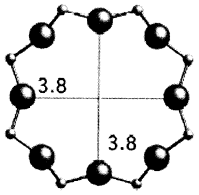


(c) SAPO-34 structure, 8-ring viewed normal to 001

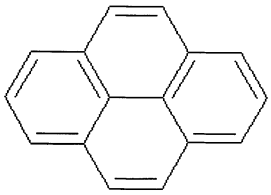

(d) Pyrene structure

**Figure 1.** Structure of microporous SAPO-5, SAPO-11, SAPO-34, and pyrene molecule.

of the adsorbates. The photophysical properties of pyrene in silica, alumina, clay, and zeolite have been the subject of numerous investigations in the laboratory of J. K. Thomas.[28−32] They reported that pyrene cation radicals are produced by irradiation with UV light and that the mechanism of photoionization on the solid can take place via a monophotonic or biphotonic process.

Although there are several reports on the photochemistry and photoionization of pyrene in several heterogeneous hosts, there are no reports on the photoionization of pyrene in microporous SAPO materials. Krishna et al. studied the photoinduced charge separation of *N*-alkylpyrene in transition metal ion containing mesoporous MCM-41 materials.[33] They observed that the stability of the photoproduced $Py_n^{+\bullet}$ was short-lived ($t_{1/2} \sim 30$ min for CuMCM-41). The low stability of $Py_n^{+\bullet}$ in MCM-41 materials suggests that they have considerable mobility within the pores. The mobility of the photoproduced cation radical is an important parameter that affects its stability. Xiang and Kevan have observed that the photoyield and stability of alkylphenothiazine cation radicals ($PC_n^{+\bullet}$) decrease with an increase in pore size, and they attributed the effect due to the increased mobility of $PC_n^{+\bullet}$ in large pore size materials.[34] Similarly, Dutta et al. have observed that constrainment and tight packing of $Ru(bpy)_3^{2+}$ in the zeolite supercage can contribute to considerable slowing of the BET reaction.[35] Recognizing this important factor, in the present investigation, we explored the photoinduced charge separation of pyrene in microporous chromium containing SAPO-5 materials. The pore opening of SAPO-5 is 7.3 Å, slightly larger than the molecular dimensions of pyrene that are 6.9 Å × 13 Å (Figure 1d). Thus, a molecule such as pyrene can be tightly fitted inside SAPO-5; such a host system can provide an appropriate spatial environment to accommodate pyrene, and we expect that the restricted mobility of the photoproduced pyrene cation radical within the pores of SAPO-5 would stabilize it.

## Experimental Section

**Synthesis of SAPO-*n* (*n* = 5, 11, 34).** The synthesis of SAPO-5 was achieved following a literature procedure.[36] In brief, aluminum isopropoxide (23.15 g, 0.11 mol, Aldrich) was slurried in 35 mL of water. Phosphoric acid (85 wt %, 13 g, 0.11 mol, Aldrich) was added to the alumina slurry and stirred for 1 h. Cyclohexylamine (4.0 g, 0.04 mol, Aldrich) was then added, and the gel was stirred for 90 min at room temperature. Silica gel (Ludox AS-40, 40 wt %, 6.0 g, 0.04 mol, Aldrich) was then added, and the mixture was stirred for a further 10 min. The gel was then placed in a Teflon-lined autoclave and heated to 473 K for 14 h under autogenous pressure. After the hydrothermal synthesis, the autoclave was quenched to room temperature and the product was separated from the mother liquor, washed well with deionized water, and then dried at 353 K in air overnight. The as-synthesized product was then slowly heated to 823 K in oxygen and kept at this temperature for 12 h in order to remove the organic template to give H−SAPO-5.

SAPO-11 was synthesized according to the literature.[37] A reaction mixture was prepared by combining 11.56 g (0.1 mol) of 85 wt % phosphoric acid (Aldrich) and 5.0 g of water with 20.42 g (0.1 mol) of aluminum isopropoxide (Aldrich) and stirred well. This mixture was added to 6.0 g (0.03 mol) of an aqueous sol containing 30 wt % of $SiO_2$ (Aldrich) and 0.8 g of water and stirred until homogeneous. Finally, 4.6 g (0.05 mol) of dipropylamine (Aldrich) was added and the mixture was stirred until homogeneous. The reaction mixture was then placed in a Teflon-lined autoclave and heated to 473 K for 48 h. After the hydrothermal synthesis, the autoclave was quenched to room temperature. The solid product was recovered, washed repeatedly with water, and dried in air at 353 K. The as-synthesized product was then slowly heated to 823 K in oxygen and kept at this temperature for 24 h in order to remove the organic template to give H−SAPO-11.

SAPO-34 was prepared by a procedure developed in our laboratory.[38] In a typical synthesis, 10 mL of water was added to 5.85 g (0.08 mol) of pseudoboehmite (Catapal-B, Vista) and then 9.3 g (0.08 mol) of phosphoric acid (Aldrich) and 10 mL of additional water were added slowly. After the mixture was stirred for 2 h, 1.4 g (0.02 mol) of fumed silica (Aldrich) and 10 mL of water were added slowly and the mixture was stirred for 30 min. Finally, 7.0 g (0.08 mol) of the template, morpholine (Aldrich), and 10 mL of water were added dropwise. The gel was stirred for 24 h at room temperature and finally placed in a Teflon-lined autoclave and heated to 473 K for 48 h. After the hydrothermal synthesis, the autoclave was quenched to room temperature. The product was recovered, washed with water several times, and then dried in air at 373 K for 12 h. The as-

synthesized product was then slowly heated to 823 K in oxygen and kept at this temperature for 14 h in order to remove the organic template and give H−SAPO-34.

**Preparation of Cr Containing SAPO-5.** Cr ions were incorporated into the SAPO-5 materials in both extraframework and framework positions. To incorporate metal ions into extraframework positions, ion exchange of protons of calcined H−SAPO-5 was done by liquid state ion exchange. Typical ion exchange was performed by adding 10 mL of $5 \times 10^{-3}$ M $Cr(NO_3)_3$ and 40 mL of water to 2 g of H−SAPO-5 and stirring the mixture (pH = 6.5) overnight at room temperature. The samples were then filtered, washed with hot distilled water to remove any excess metal ions on the surface of the sample, and then dried in air. The samples prepared in this manner are designated as CrH−SAPO-5. Two ion-exchanged samples were prepared. The first one was heated at 100 °C and was designated as Cr(III)H−SAPO-5. The second sample was heated slowly up to 500 °C and cooled slowly to room temperature and was designated as Cr(V)H−SAPO-5. ESR results show that Cr exists as Cr(V) in this sample, as discussed later. Cr containing ions in the framework was prepared as described for SAPO-5, except that a required amount of $CrCl_3$ was introduced into the synthesis gel. The Cr containing samples were then calcined and were designated as CrAPSO-5.

**Pyrene Incorporation.** A typical procedure for incorporation of pyrene is as follows. Py was incorporated by immersing 0.1 g of the SAPO sample in 1 mL of $5 \times 10^{-3}$ M Py in benzene for 12 h in the dark. Benzene was removed by flowing nitrogen gas for 1 h in the dark. For ESR measurements, 0.1 g of the SAPO-5 sample was transferred into Suprasil quartz tubes (2 mm i.d. × 3 mm o.d.) that were sealed at one end. The pyrene cation radical yield and stability were strongly affected by the presence of adsorbed water and oxygen. For samples that were not evacuated to remove traces of oxygen, solvent (benzene), and adsorbed water molecules, the pyrene cation radical yield was found to decrease after 10 min of irradiation. Thus, any such impurities seem to affect the results and further photoionization experiments were carried out with evacuation below 1 Torr. An optimum time of 8 h was found to be necessary for evacuation. For diffuse reflectance spectroscopy (DRS) studies, the samples were loaded into a cylindrical quartz sample cell (22 mm diameter × 20 mm path length) and evacuated for 8 h prior to irradiation. The amount of pyrene incorporated into the pores of the SAPO materials was measured optically from the decrease of pyrene in the liquid.

**Characterization.** X-ray diffraction powder patterns were recorded on a Siemens 5000 X-ray diffractometer using Cu Kα radiation of wavelength 1.541 Å in the range $10° < 2\theta < 50°$. Chemical analysis was performed by electron microprobe analysis (EMPA) on a JEOL JXA-8600 spectrometer. The composition of the SAPO materials was determined by calibration with known standards and by averaging over several defocused areas to give the bulk composition. ESR spectra were recorded at room temperature at 9.5 GHz using a Bruker ESP 300 spectrometer with a 100 kHz field modulation and low microwave power to avoid power saturation. Photoproduced $Py^{+\bullet}$ yields were determined by double integration of the ESR spectra using the ESP 300 software. Each photoyield is an average of three ESR scans with a precision of less than 4%. The DRS were recorded at room temperature using a Perkin-Elmer 330 model spectrophotometer equipped with an integrating sphere. Thermal gravimetric analysis (TGA) of the samples was performed using a TGA 2050 analyzer (TA instruments) in oxygen atmosphere at a heating rate of 10 °C/min.

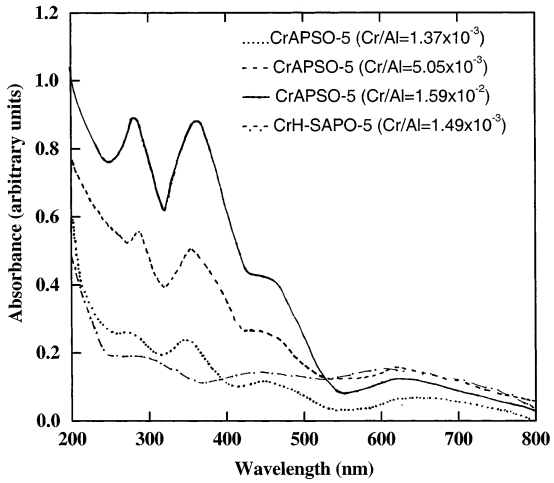


**Figure 2.** Diffuse reflectance spectra of CrAPSO-5 and Cr(III)H−SAPO-5 samples.

**Photoirradiation.** The Py containing SAPO materials were irradiated using a 300 W Cermax Xenon lamp (ILC-LX 300 UV) at room temperature. The incoming light was passed through a 10 cm water filter to prevent infrared radiation and through a Corning No. 7-54 filter to give light of $\sim 1 \times 10^6$ erg $cm^{-2}$ $s^{-1}$ intensity with a maximum wavelength at 320 ± 20 nm. The samples, sealed in a quartz tube, were placed in a quartz Dewar and rotated at a speed of 4 rpm to ensure even irradiation.

## Results

**X-ray Powder Diffraction.** The XRD powder patterns of the as-synthesized and calcined SAPO-5, SAPO-11, and SAPO-34 show them to be highly crystalline and in good agreement with literature reports. A good baseline obtained confirms good crystallinity for all of the calcined CrAPSO-5 and ion-exchanged CrH−SAPO-5 samples. EMPA shows that chromium is homogeneously dispersed in the SAPO-5 samples. However, it was noted that the sample crystallinity of SAPO-11 and SAPO-34 was reduced by ∼25 and ∼10% after calcination.

**UV−vis Spectra.** The oxidation state and coordination environment of Cr can be identified from a combination of techniques such as ESR and DRS. It has been observed that the oxidation state and the local coordination of Cr are strongly dependent on the pretreatment conditions and on the nature and composition of the support.[39−43] The type and relative concentration of Cr species formed are therefore treatment-, loading-, and support-dependent. Zhu and Kevan have observed that Cr(V) is the predominant species formed in calcined CrAPSO-11 and CrAPSO-5.[44,45] Similarly, Cr(V) has been identified as the main species in CrAPO-5 samples calcined in air at 550 °C.[46,47] Figure 2 shows the DR spectra of the calcined CrAPSO-5 samples and the ion exchanged CrH−SAPO-5 sample. The spectra of the calcined CrAPSO-5 show four bands near 280, 350, and 450 nm and a broad band centered around 620 nm. The intensities of the band increase monotonically with an increase in Cr content. The bands in the UV region (280 and 350 nm) are normally assigned to charge transfer transitions associated with Cr(VI). However, $O \rightarrow Cr^{5+}$ charge transfer bands also occur in the same region. The bands observed in the UV region in Cr(V) doped $Ca_2PO_4Cl$, vanadates, and phosphates have been assigned to $O \rightarrow Cr^{5+}$ charge transfer bands.[48−50] The ESR studies described later also suggest that Cr(V) is present in the calcined samples. Thus, we assign the two optical bands in the UV region to Cr(V) formed by oxidation of Cr(III) during calcination consistent with previous

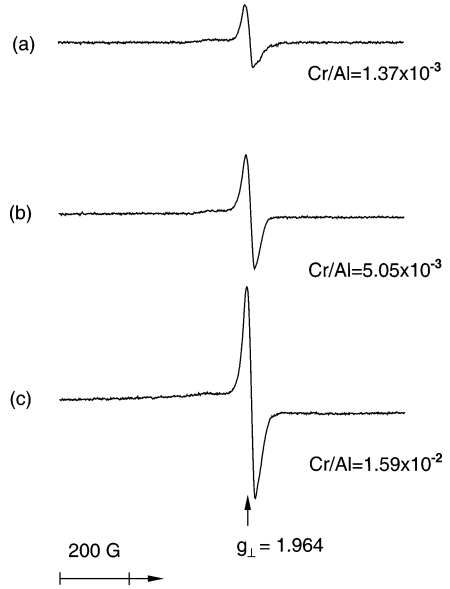


**Figure 3.** Room temperature ESR spectra of CrAPSO-5: (a) Cr/Al = $1.37 \times 10^{-3}$, (b) Cr/Al = $5.05 \times 10^{-3}$, and (c) Cr/Al = $1.59 \times 10^{-2}$.

reports from our laboratory.[18,44,45] The two bands in the visible region observed near 450 and 620 nm for CrAPSO-5 are typically assigned to d−d transitions of Cr(III) either in an octahedral or in a distorted octahedral environment. These are assigned to $^4A_{2g} \rightarrow {}^4T_{1g}$ and $^4A_{2g} \rightarrow {}^4T_{2g}$ transitions. These transitions can be due to $Cr_2O_3$ clusters or due to isolated Cr(III) ions. Thus, on calcination, most of the Cr(III) ions are oxidized to Cr(V) in CrAPSO-5. For Cr(III)H−SAPO-5, the observed bands are in accordance with literature reports of octahedral Cr(III) species.[39]

**ESR Spectra.** The ESR spectra of liquid state ion-exchanged Cr(III)H−SAPO-5 (not shown) prior to calcination show a very broad signal at $g = 1.97$ assigned to $Cr^{3+}$ consistent with earlier reports.[44] The ion-exchanged sample calcined at 500 °C, Cr(V)H−SAPO-5, shows a sharp signal at $g = 1.967$ assigned to $Cr^{5+}$. The calcined CrAPSO-5 samples show a sharp signal at $g = 1.964$. This signal is assigned to a $g_\perp$ component of $Cr^{5+}$ possibly in either a distorted octahedral or a square pyramidal coordination. The expected $g_{||}$ component at ∼1.95 is normally a very weak absorption shape signal and weak to be observed at room temperature. The lack of resolution may be due to a $g$ strain broadening process or due to the spin exchange effect as discussed by Dalal et al.[51] Figure 3 shows the room temperature ESR spectra of the calcined CrAPSO-5 samples. From Figure 3, we can see that the intensity of the signal at $g = 1.964$ increases with Cr content, while the line width does not change with Cr content. When the ESR experiments were carried out at 77 K, two signals were observed, a sharp signal at $g = 1.964$ and a very weak shoulder at $g = 1.941$. This weak shoulder is assigned to a $g_{||}$ component. The line width and shape of the ESR signals observed in the present study are similar to the ones observed in previous studies.[44,45] According to the $g$ formulas[52] for square pyramidal geometry, $g_\perp = g_e - 2\lambda/\Delta_0$ and $g_{||} = g_e - 8\lambda/\Delta_1$ where $\lambda$ is the spin−orbit coupling constant of 160 $cm^{-1}$ for Cr(V) in an oxide environment and $\Delta_0$ and $\Delta_1$ are the two lowest energy UV transitions for calcined CrAPSO-5. The calculated $g$ values are $g_\perp = 1.97$ and $g_{||} = 1.951$, which is in close agreement with the observed values of $g_\perp = 1.964$ and $g_{||} = 1.941$. These results thus seem to support the assignments of the ESR spectrum to square pyramidal Cr(V). Hydrated Cr(V) containing compounds such as $Li_3CrO_8$, $Cs_3CrO_8$, and $Na_3CrO_8$ also show $g_\perp > g_{||}$.[53] Similar assignments

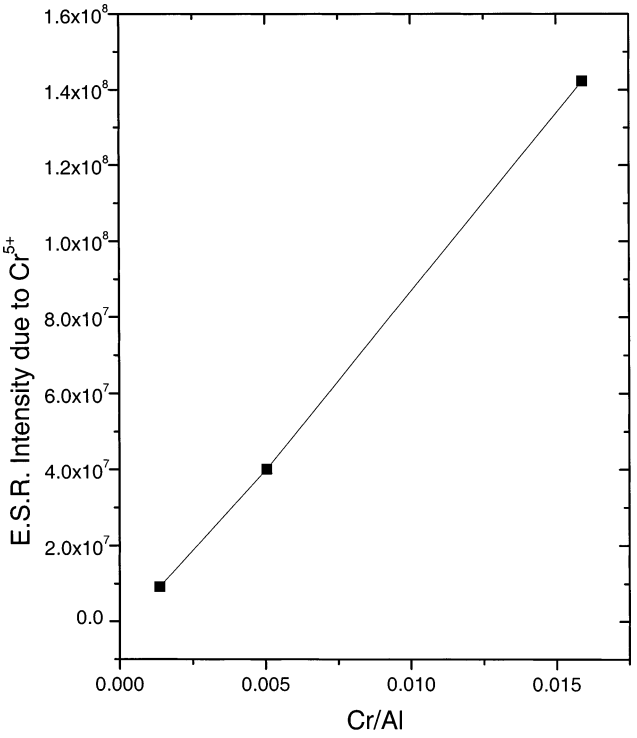


**Figure 4.** Intensity of ESR signal due to Cr(V) vs Cr content in calcined CrAPSO-5 samples.

of Cr(V) in square pyramidal coordination on various supports with $g_\perp \sim 1.97$ and $g_{||} \sim 1.94$ have been reported by several authors.[15,41,44,45] For octahedral geometry, $g_\perp < g_{||}$, which does not agree with the experimental $g$ values. Furthermore, the fact that $g_\perp > g_{||}$ suggests that the ground state may be $d_{x^2-y^2}$ than $d_{z^2}$. Also consistent with the Cr(V) assignment is the fact that the ESR signal at $g = 1.964$ due to Cr(V) increases with Cr content as shown in Figure 4.

**Photoionization Studies.** The photoyield of pyrene was found to be dependent on the evacuation conditions and pyrene concentration. The stability of the photoproduced $Py^{+\bullet}$ was found to be short-lived ($t_{1/2} \sim 20$ min) for samples that were not evacuated. Also, the sample changed color from white to gray, indicative of the formation of photooxygenated product(s). Reyes et al. have similarly observed that irradiation of pyrene adsorbed on silica in the presence of oxygen led to the formation of oxidized products such as 1,6-pyrenedione and 1,8-pyrenedione in addition to small amounts of 1-hydroxypyrene.[54] Samples subjected to evacuation showed no such change in color, and the $Py^{+\bullet}$ yield was significantly higher. The pyrene cation radical yield ($Py^{+\bullet}$) was found to increase up to 8 h of evacuation, and a further increase in evacuation time was found to essentially give the same photoyield; hence, all samples were subjected to evacuation for 8 h.

The photoyield of $Py^{+\bullet}$ was found to depend on the concentration of pyrene. The maximum photoyield was found to be for a pyrene concentration of $5 \times 10^{-3}$ M. At this concentration, the loading of pyrene corresponds to 5 $\mu$mol/g. At concentrations greater than $5 \times 10^{-3}$ M, the photoyield of $Py^{+\bullet}$ was found to decrease. The loading of pyrene in SAPO-5 was measured to be 10, 15, and 18 $\mu$mol/g at pyrene concentrations of $1 \times 10^{-2}$, $5 \times 10^{-2}$, and $1 \times 10^{-1}$ M, respectively. The drop in the yield of $Py^{+\bullet}$ may be attributed to the presence of ground state pairs and/or aggregates (formed as loading is increased), which can act as a light sink to absorb the incident light without inducing any photochemistry. Photoionization of pyrene was examined in different SAPO materials to study the

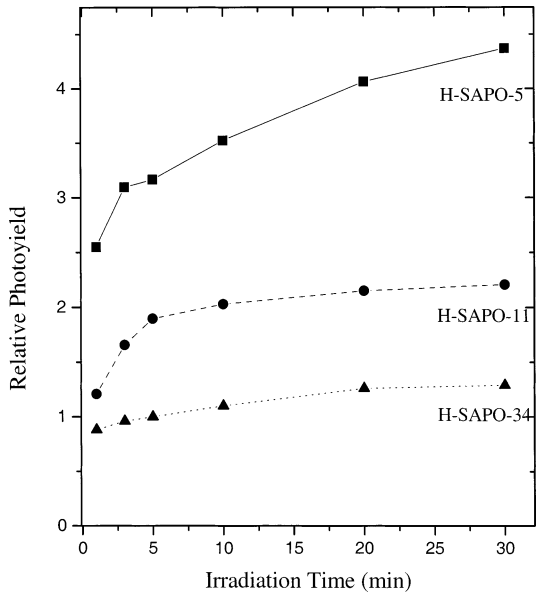


**Figure 5.** Room temperature photoinduced $Py^{+\bullet}$ cation radical yield measured by ESR vs irradiation time for H−SAPO-5, H−SAPO-11, and H−SAPO-34.

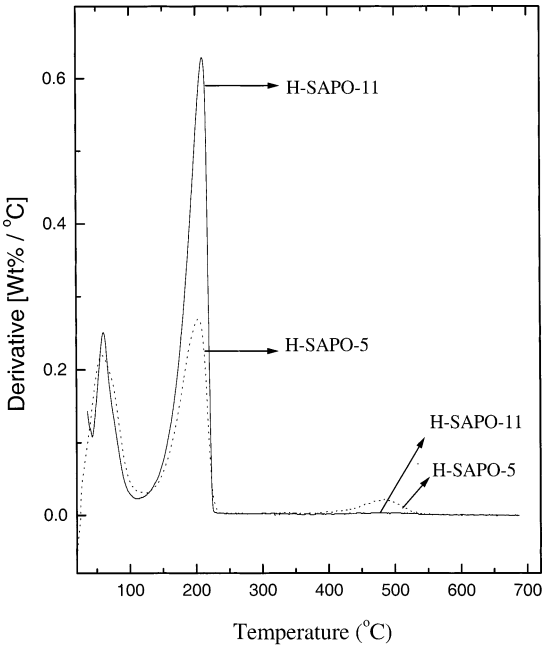


**Figure 6.** TGA of H−SAPO-5, H−SAPO-11, and H−SAPO-34 with impregnated pyrene.

effect of pore size, and the results are shown in Figure 5. As can be observed from Figure 5, the photoyield of $Py^{+\bullet}$ decreases in the order H−SAPO-5 > H−SAPO-11 > H−SAPO-34. The observed trend suggests that the entry of pyrene molecules is restricted in the channels of SAPO-11 and SAPO-34. The results from the thermal gravimetric studies are shown in Figure 6. Figure 6 shows the TG studies of pyrene incorporated in H−SAPO-5 and H−SAPO-11. The curve shows three weight losses: the first near 60 °C is attributed to water desorption, the second near 200 °C is attributed to pyrene desorption, and the third broad peak centered around 500 °C is assigned to the decomposition of pyrene in an oxygen atmosphere within the pores. This peak is not observed when the experiments are carried out in an inert atmosphere. For SAPO-11, we see only two peaks, a peak near 60 °C due to water desorption and the second near 200 °C due to pyrene desorption. The intensity of

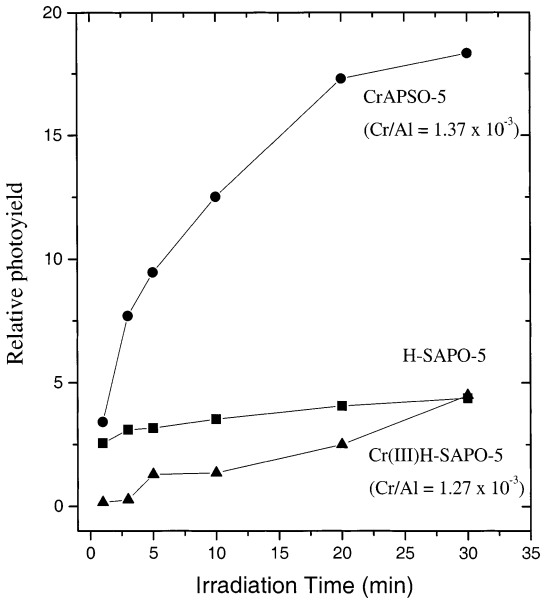


**Figure 7.** Room temperature photoinduced $Py^{+\bullet}$ cation radical yield measured by ESR vs irradiation time for H−SAPO-5, Cr(III)H−SAPO-5, and CrAPSO-5.

the peak ∼200 °C is higher in SAPO-11 than in SAPO-5 suggesting that pyrene is predominantly adsorbed on the surface of SAPO-11. A similar behavior was exhibited by SAPO-34 and is not shown for the sake of clarity. Thus, TG studies indicate that SAPO-5 can accommodate pyrene whereas the pore opening of SAPO-11 and SAPO-34 restricts the entry of pyrene molecules. The low photoyield of $Py^{+\bullet}$ observed in SAPO-11 and SAPO-34 may be due to pyrene molecules adsorbed on their surface.

We have earlier observed that Cr containing SAPO-5 and zeolite X show higher yields of methylphenothiazine and *N*,*N*,*N*′,*N*′-tetramethylbenzidine cation radical as compared to other transition metal ion containing microporous materials.[15,18,55] Thus, it is of interest to study the photoionization of pyrene in Cr containing SAPO-5 materials. The ESR spectra of pyrene-impregnated Cr(III) liquid state ion-exchanged SAPO-5 show a signal at $g = 2.003$ due to $Py^{+\bullet}$ assigned to pyrene cation radical prior to irradiation. This means that some $Py^{+\bullet}$ is produced in the dark during sample preparation. No ESR signal at $g \sim 2.00$ is observed for samples that are irradiated and that do not contain pyrene; hence, pyrene is the only photosensitive molecule in these systems. The ESR spectra of CrAPSO-5/Py show a signal at $g = 1.964$ due to Cr(V) as discussed earlier. On impregnation of Py (prior to irradiation), a new signal at $g = 2.003$ assigned to $Py^{+\bullet}$ is seen. After it is irradiated by 320 nm light at room temperature for 5 min, the samples showed strong ESR signals. With a further increase in irradiation time, the intensity of the ESR signal further increases and reaches a plateau in about 30 min. Figure 7 shows the changes in the ESR intensity of the ESR signal due to $Py^{+\bullet}$ in H−SAPO-5, Cr(III)H−SAPO-5, and in CrAPSO-5. The highest yield is obtained for CrAPSO-5. The photoyield and stability of $Py^{+\bullet}$ were found to decrease in the order CrAPSO-5 > Cr(III)H−SAPO-5 > H−SAPO-5. The photoyield of $Py^{+\bullet}$ after 30 min of irradiation is similar for H−SAPO-5 and CrH−SAPO-5(l). However, the net photoyield (after subtracting the dark yield) is higher in CrH−SAPO-5(l). This suggests that the Cr ion containing SAPO-5 materials are better hosts for forming and stabilizing $Py^{+\bullet}$ cation radicals. Furthermore, Cr(V) containing SAPO-5 exhibits a higher photoyield and stability toward $Py^{+\bullet}$. Also, it was found that the yield of $Py^{+\bullet}$ was approximately

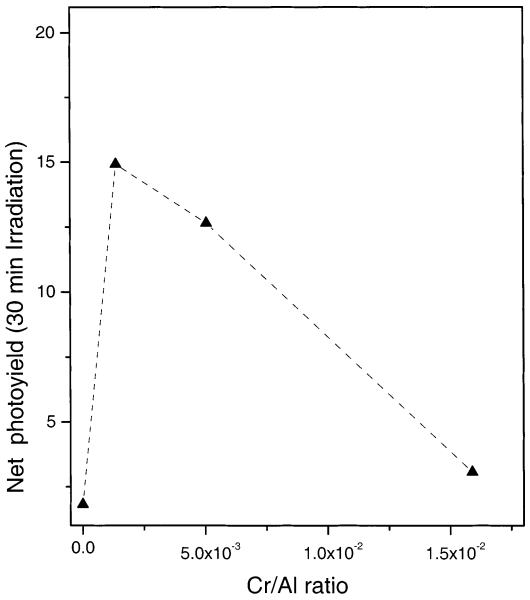


**Figure 8.** Room temperature photoinduced $Py^{+\bullet}$ cation radical yield measured by ESR vs Cr/Al ratio for CrAPSO-5 samples.

twice higher in CrAPSO-5 than in Cr(V)H−SAPO-5. The reason for the lower activity may be due to the fact that the extraframework Cr ions partially block the access of pyrene molecules into the pore. This is substantiated by the fact that the loading of pyrene was found to be ~2.3 $\mu$mol/g in Cr(V)H−SAPO-5 as compared to ~5.2 $\mu$mol/g in CrAPSO-5.

To understand the influence of the Cr content on the photoyield and stability of $Py^{+\bullet}$, CrAPSO-5 samples were prepared with different Cr/Al ratios. The results obtained from the photoionization of pyrene in CrAPSO-5 are shown in Figure 8. It is evident from the figure that the photoyield of $Py^{+\bullet}$ decreases with an increase in Cr concentration. The dark yield of $Py^{+\bullet}$ was found to increase with an increase in Cr content. The relative dark yields are 3.05 for CrAPSO-5 (Cr/Al = $1.37 \times 10^{-3}$), 3.5 for CrAPSO-5 (Cr/Al = $5.05 \times 10^{-3}$), and 4.3 for CrAPSO-5 (Cr/Al = $1.59 \times 10^{-2}$). The photoyield after 30 min of irradiation was found to be more or less similar in all CrAPSO-5 samples. Thus, the net photoyield (note that the dark reaction must be subtracted from the photoyield to obtain the net photoyield) decreases as the Cr content increases.

Figure 9 shows the ESR spectra of CrAPSO-5 (Cr/Al = $1.37 \times 10^{-3}$) before incorporation of pyrene and after UV irradiation of CrAPSO-5/Py (Cr/Al = $1.37 \times 10^{-3}$) for 30 min. The ESR spectra show two signals: one at $g = 2.003$ due to $Py^{+\bullet}$ and another at $g = 1.964$ due to Cr(V) as discussed earlier. The ESR signals due to $Py^{+\bullet}$ and Cr(V) partially overlap. Thus, a direct measurement of the signal intensity for the $Py^{+\bullet}$ cation radical by double integration is not precise. The relative intensity of the $Py^{+\bullet}$ cation radical was measured in the following manner for these samples. The signals before irradiation were subtracted from the signals after irradiation, and the relative intensity of $Py^{+\bullet}$ was estimated from the height of the resulting line at $g = 2.003$. This method of calculating the relative intensity of the photoproduced $Py^{+\bullet}$ seems fairly reliable since the height of the signal at $g = 2.003$ gives an approximate measure of the amount of $Py^{+\bullet}$. From Figure 9, we can see that there is an increase in the relative intensity of the peak at $g = 2.003$ and a decrease in the relative intensity of the peak at $g = 1.964$ after 30 min of irradiation. The ESR studies thus seem to suggest that Cr(V) acts as an electron acceptor. In addition, the photoproduced $Py^{+\bullet}$ cation radical is stable for weeks in the dark at room temperature. The half-life of $Py^{+\bullet}$ is estimated to

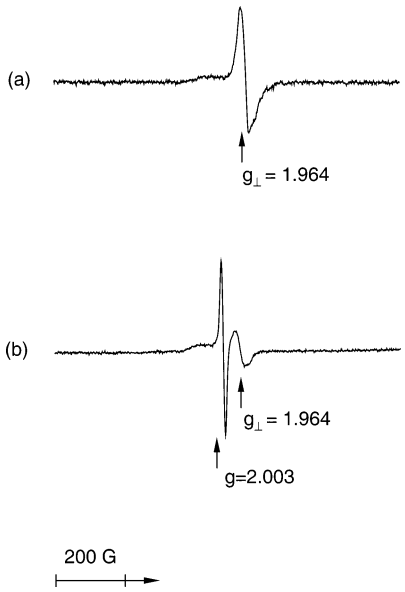


**Figure 9.** ESR spectra of CrAPSO-5 (Cr/Al = $1.37 \times 10^{-3}$) before incorporation of pyrene and CrAPSO-5/Py (Cr/Al = $1.37 \times 10^{-3}$) upon UV irradiation at 320 nm for 30 min.

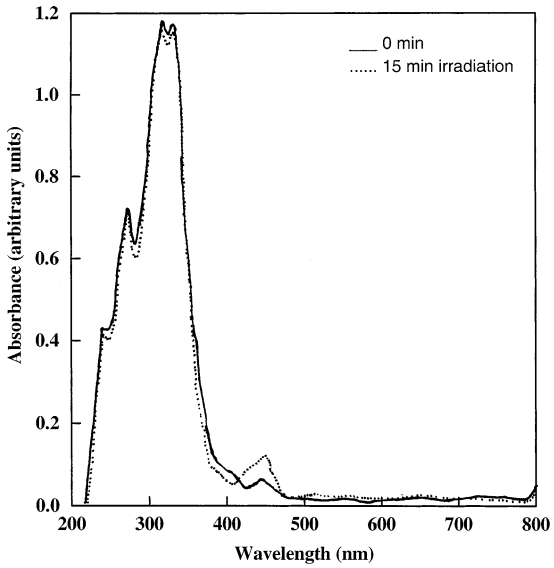


**Figure 10.** Diffuse reflectance spectra of CrAPSO-5/Py (Cr/Al = $1.37 \times 10^{-3}$) at room temperature upon UV irradiation.

be ~45 days in CrAPSO-5. This is a marked improvement over the stability of $Py^{+\bullet}$ in mesoporous MCM-41 materials where the half-life of $Py^{+\bullet}$ ranged from 5 to 30 min.[33]

A DRS study of CrAPSO-5/Py (Cr/Al = $1.37 \times 10^{-3}$) before and after irradiation is shown in Figure 10. The absorption spectra in the UV region show structured absorption bands typical of pyrene in polar solutions. In addition, there is a small peak at 450 nm assigned to $Py^{+\bullet}$. This is consistent with ESR studies that indicate that $Py^{+\bullet}$ cation radicals are formed prior to irradiation. The spectrum compares well with the reported absorption spectrum of pyrene in homogeneous solution. After irradiation, there is a small decrease in the absorption due to pyrene and an increase in the absorption at 450 nm due to $Py^{+\bullet}$. The DR spectra of other Cr containing CrAPSO-5/Py samples also showed a similar behavior.

## Discussion

The ESR and DRS results suggest that Cr is present predominantly as Cr(III) in the as-synthesized sample and is

oxidized mainly to Cr(V) in the calcined samples in addition to some amount of Cr(III). On the basis of the ESR and DRS results and other reports of Cr(V) in CrAPSO-5 and in phosphate and vanadate hosts,[48−50] the bands in the UV region are assigned to O → Cr(V) charge transition. Furthermore, the ESR studies indicate that the geometry of Cr(V) ions is most probably a square pyramidal coordination.

The photooxidation of pyrene into pyrene cation radical is confirmed by the ESR and DRS results. The yield of $Py^{+\bullet}$ was found to increase linearly with light intensity. The low intensities of light used in the study indicate that the ionization process is a monophotonic process. The TGA studies indicate that pyrene could be incorporated into the pores of H−SAPO-5 and not in H−SAPO-11 and H−SAPO-34. The typical concentration of pyrene reported in this study is 10 mg of pyrene per g of SAPO-5. For a surface area of ∼200 $m^2$/g for SAPO-5, there would be one molecule of pyrene in an area of ∼670 $Å^2$. This shows that the coverages of pyrene in the SAPO-5 samples are far less than monolayer coverages. Mao and Thomas[56] observed that at higher loadings, in addition to $Py^{+\bullet}$, dimer radical cation ($Py_2^{+\bullet}$) is also formed. In the present study, the ESR results did not indicate the formation of such species ($Py_2^{+\bullet}$). To confirm the absence of this species, DRS studies were carried out in the near-IR region. The dimer aromatic radical cation of pyrene is characterized by a broad absorption band near 1400 nm. However, the DRS studies in the near-IR region did not reveal the presence of any such band in this region. Thus, the results obtained in the present study are quite different from the results obtained by Mao and Thomas in the failure to detect species such as $Py_2^{+\bullet}$ at higher loadings. At higher coverages, the pyrene molecules may form ground state pairs and/or aggregates; hence, the pyrene cation radical yield decreases. Similarly, Reyes et al.[54] have observed that the photodegradation rate of pyrene adsorbed on silica drops significantly at higher surface coverages. They attributed this to the formation of ground state pairs and/or aggregates.

The pore size is a critical parameter affecting the photoyield of the radical cation and its stability. This is related to the control of the spatial separation between the electron acceptor and the electron donor. The photoionization experiments show that the photoyield and the stability of the $Py^{+\bullet}$ are highest in H−SAPO-5 as compared to H−SAPO-11 and H−SAPO-34. The H−SAPO-5/Py samples show weak ESR signals after 30 min of irradiation, suggesting that the protons in H−SAPO-5 may act as electron acceptors. Low-temperature measurements at 77 K were made to detect trapped hydrogen atoms, but none were seen. ESR signals due to hydrogen atoms were observed only in large pore silica, and this is consistent with the present results.[56]

The ESR and DRS results clearly confirm the photooxidation of pyrene molecules to $Py^{+\bullet}$ cation radicals at room temperature. The increase in the intensity of the signal at $g = 2.003$ due to $Py^{+\bullet}$ with time for the Cr containing SAPO-5 samples suggests that the Cr ions, especially Cr(V) ions, assist in the formation and stabilization of the pyrene cation radicals. The ESR studies indicate that Cr(V) acts as an electron acceptor. The dark reaction yield increases as the Cr content increases suggesting the role of Cr(V) ions as electron acceptors. After 30 min of irradiation, there is an increase in the relative intensity of the signal at $g = 2.003$ and a decrease in the relative intensity of the signal at $g = 1.964$ due to Cr(V) (not shown) as indicated by eq 1.

$$\mathrm{Cr(V)} + \mathrm{Py} \rightarrow \mathrm{Cr(IV)} + \mathrm{Py}^{+\bullet} \qquad (1)$$

Also, when CrAPSO-5/Py samples are stored in the dark after irradiation, the relative intensity of the signal at $g = 1.964$ slowly increases and simultaneously the relative intensity of the signal at $g = 2.003$ slowly decreases in accordance with the BET reaction. These points suggest that Cr(V) ions act as the electron acceptor and assist in stabilizing the photoproduced $Py^{+\bullet}$ cation radical. The photoyield and stability of $Py^{+\bullet}$ in Cr(V) containing SAPO-5 samples are higher than in Cr(III) samples suggesting that the electron affinity of Cr plays an important role. This can be explained on the basis of the higher electron affinity of Cr(V) ($E°$ $Cr^{5+}/Cr^{4+} = 1.340$ V) as compared to Cr(III) ($E°$ $Cr^{3+}/Cr^{2+} = -0.407$ V).[58] The reduction potential of Cr(V) is positive making the reaction more favorable than that of Cr-(III). The dark yield of $Py^{+\bullet}$ increases in the order Cr(III) > H > Cr(V) in SAPO-5 microporous materials in accordance with the increase in the standard reduction potentials. The fact that Cr(V) containing SAPO-5 exhibits remarkable stability toward $Py^{+\bullet}$ suggests that the standard potential of the transition metal ion $M^{n+/(n-1)+}$ may be used as a guide for designing systems with increased efficiency.

The stability of the photoproduced $Py^{+\bullet}$ is higher in CrAP-SO-5 ($t_{1/2} \sim 45$ days) as compared to other systems investigated in our laboratory and other reports in the literature.[29,33] Thus, the photooxidation mechanism in CrAPSO-5 is more efficient than in other oxide hosts.

## Conclusions

Cr containing SAPO-5 microporous materials were investigated for the photoionization of pyrene. The pyrene cation radical yield was found to depend on the electron affinity, on the Cr content, and on the pore size of the host. ESR studies indicate that Cr(V) is an electron acceptor. The stability of the photoproduced $Py^{+\bullet}$ is found to be longer than in other oxide hosts. This is attributed to the constrainment and the tight fitting of the pyrene molecules in the SAPO-5 pores. Thus, Cr(V) containing SAPO-5 microporous materials provide an appropriate electronic and spatial environment to minimize the BET reaction and prolong the lifetime of the photogenerated $Py^{+\bullet}$ for many weeks at room temperature.

**Acknowledgment.** This research was supported by the Chemical Sciences, Geosciences, and Biosciences Division, Office of the Basic Energy Sciences, Office of Science, U.S. Department of Energy. K.T.R. thanks Prof. Allan J. Jacobson for useful discussions and review of the manuscript.

## References and Notes

(1) Scaiano, J. C.; Garcia, H. *Acc. Chem. Res.* **1999**, *32*, 783.
(2) Kincaid, J. R. *Chem. Eur. J.* **2000**, *6*, 4055.
(3) Gust, D.; Moore, T. A.; Moore, A. L. *Acc. Chem. Res.* **2001**, *34*, 40.
(4) *Advances in Photosynthesis*; Govindjee, Ed.; Kluwer Academic Publishers: Dordrecht, 2001.
(5) Photochemistry in Organized and Constrained Media; Ramamurthy, V., Ed.; VCH: New York, 1991.
(6) Dutta, P. K.; Borja, M. *Nature* **1993**, *362*, 43.
(7) Corma, A.; Fornes, V.; Galletero, M. S.; Garcia, H.; Scaiano, J. C. *Chem. Commun.* **2002**, 334.
(8) Vermeulen, L. A.; Thompson, M. E. *Nature* **1992**, *358*, 656.
(9) Alkaitis, S. A.; Beck, G.; Grätzel, M. *J. Am. Chem. Soc.* **1975**, *97*, 5723.
(10) Kang, Y. S.; Kevan, L. *J. Phys. Chem.* **1994**, *98*, 4389.
(11) Matsuura, K.; Kevan, L. *J. Phys. Chem.* **1996**, *100*, 10652.
(12) Narayana, P. A.; Li, A. S. W.; Kevan, L. *J. Am. Chem. Soc.* **1982**, *104*, 6502.
(13) Xiang, B.; Kevan, L. *Colloids Surf. A* **1993**, *72*, 11.
(14) Stenland, C.; Kevan, L. *J. Phys. Chem.* **1993**, *97*, 10498.
(15) Ranjit, K. T.; Kevan, L. *Phys. Chem. Chem. Phys.* **2001**, *3*, 2921.

(16) Bae, J. Y.; Kevan, L. *Microporous Mesoporous Mater*. **2001**, *50*, 1.
(17) Kurshev, V.; Prakash, A. M.; Krishna, R. M.; Kevan, L. *Microporous Mesoporous Mater*. **2000**, *34*, 9.
(18) Ranjit, K. T.; Kevan, L. *J. Phys. Chem. B* **2002**, *106*, 9306.
(19) Turro, N. J.; Garcia-Garibay, M. A. In *Photochemistry in Organized and Constrained Media*; Ramamurthy, V., Ed.; VCH: New York, 1991; pp 1−38.
(20) Cozens, F. L.; Garcia, H.; Scaiano, J. C. *Langmuir* **1994**, *10*, 2246.
(21) Cano, M. L.; Cozens, F. L.; Garcia, H.; Marti, V.; Scaiano, J. C. *J. Phys. Chem.* **1996**, *100*, 18152.
(22) Hartmann, M.; Kevan, L. *Chem. Rev.* **1999**, *99*, 635.
(23) Hartmann, M.; Kevan, L. *J. Phys. Chem.* **1996**, *100*, 4606.
(24) Behymer, T. D.; Hites, R. A. *Environ. Sci. Technol.* **1988**, *22*, 1311.
(25) Dabestani, R.; Ellis, K. J.; Sigman, M. E. *J. Photochem. Photobiol. A* **1995**, *86*, 231.
(26) Dabestani, R.; Nelson, M.; Sigman, M. E. *Photochem. Photobiol.* **1996**, *64*, 80.
(27) Zingg, S. P.; Sigman, M. E. *Photochem. Photobiol.* **1993**, *57*, 453.
(28) Liu, X.; Iu, K.-K.; Thomas, J. K. *J. Phys. Chem.* **1989**, *93*, 4120.
(29) Iu, K.-K.; Liu, X.; Thomas, J. K. *Chem. Phys. Lett.* **1991**, *186*, 198.
(30) Iu, K.-K.; Thomas, J. K. *J. Phys. Chem.* **1991**, *95*, 506.
(31) Pankasem, S.; Thomas, J. K. *J. Phys. Chem.* **1991**, *95*, 6990.
(32) Liu, X.; Iu, K.-K.; Thomas, J. K. *J. Phys. Chem.* **1994**, *98*, 7877.
(33) Krishna, R. M.; Kevan, L. *Phys. Chem. Chem. Phys.* **2001**, *3*, 5348.
(34) Xiang, B.; Kevan, L. *Langmuir* **1994**, *10*, 2688.
(35) Vitale, M.; Castagnola, N. B.; Ortins, N. J.; Brooke, J. A.; Vaidyalingam, A.; Dutta, P. K. *J. Phys. Chem. B* **1999**, *103*, 2408.
(36) Young, D.; Davis, M. E. *Zeolites* **1991**, *11*, 277.
(37) Wilson, S. T.; Lok, B. M.; Flanigen, E. M. U.S. Patent 4,310,440, 1982.
(38) Djieugoue, M.-A.; Prakash, A. M.; Kevan, L. *J. Phys. Chem. B* **1998**, *102*, 4386.
(39) Weckhuysen, B. M.; De Ridder, L. M.; Schoonheydt, R. A. *J. Phys. Chem.* **1993**, *97*, 4756.
(40) Weckhuysen, B. M.; Verberckmoes, An A.; Buttiens, An L.; Schoonheydt, R. A. *J. Phys. Chem.* **1994**, *98*, 579.
(41) Weckhuysen, B. M.; De Ridder, L. M.; Grobet, P. J.; Schoonheydt, R. A. *J. Phys. Chem.* **1995**, *99*, 320.
(42) Weckhuysen, B. M.; Schoofs, B.; Schoonheydt, R. A. *J. Chem. Soc., Faraday Trans.* **1997**, *93*, 2117.
(43) Weckhuysen, B. M.; Wachs, I. E.; Schoonheydt, R. A. *Chem. Rev.* **1996**, *96*, 3327.
(44) Zhu, Z.; Kevan, L. *Phys. Chem. Chem. Phys.* **1999**, *1*, 199.
(45) Zhu, Z.; Wasowicz, T.; Kevan, L. *J. Phys. Chem. B* **1997**, *101*, 10763.
(46) Padlyak, B. V.; Kornatowski, J.; Zadrozna, G.; Rozwadowski, M.; Gutsze, A. *J. Phys. Chem. A* **2000**, *104*, 11837.
(47) Kornatowski, J.; Zadrozna, G.; Rozwadowski, M.; Zibrowius, B.; Marlow, F.; Lercher, J. A. *Chem. Mater.* **2001**, *13*, 4447.
(48) Banks, E.; Greenblatt, M.; Holt, S. *J. Chem. Phys.* **1968**, *49*, 1431.
(49) Simo, C.; Banks, E.; Holt, S. L. *Inorg. Chem.* **1970**, *9*, 183.
(50) Milstein, J. B.; Ackerman, J.; Holt, S. L.; McGarvey, B. R. *Inorg. Chem.* **1972**, *11*, 1178.
(51) Cage, B.; Hassan, A. K.; Pardi, L.; Krzystek, J.; Brunel, L.-C.; Dalal, N. S. *J. Magn. Reson.* **1997**, *124*, 495.
(52) Kivelson, D.; Lee, S. K. *J. Chem. Phys.* **1964**, *41*, 1896.
(53) Cage, B.; Geyer, W.; Abboud, K. A.; Dalal, N. S. *Chem. Mater.* **2001**, *13*, 871.
(54) Reyes, C. A.; Medina, M.; Crespo-Hernandez, C.; Cedeno, M. Z.; Arce, R.; Rosario, O.; Steffenson, D. M.; Ivanov, I. N.; Sigman, M. E.; Dabestani, R. *Environ. Sci. Technol.* **2000**, *34*, 415.
(55) Ranjit, K. T.; Chang, Z.; Krishna, R. M.; Prakash, A. M.; Kevan, L. *J. Phys. Chem. B* **2000**, *104*, 7981.
(56) Mao, Y.; Thomas, J. K. *Langmuir* **1992**, *8*, 2501.
(57) Xiang, B.; Kevan, L. *Langmuir* **1994**, *10*, 2688.
(58) *Handbook of Chemistry and Physics*, 80th ed.; Lide, D. R., Ed.; CRC: Boca Raton, FL, 1999; pp 8−22.